NOTE

An analytical solution to proton Bragg peak deflection in a magnetic field

IOP Publishing Physics in Medicine and Biology

Phys. Med. Biol. **57** (2012) N329–N337 doi:10.1088/0031-9155/57/17/N329

NOTE

An analytical solution to proton Bragg peak deflection in a magnetic field

Russell Wolf and Thomas Bortfeld

Department of Radiation Oncology, Massachusetts General Hospital and Harvard Medical School, 30 Fruit St, Boston, MA 02114, USA

Received 30 March 2012, in final form 12 July 2012
Published 15 August 2012
Online at stacks.iop.org/PMB/57/N329

Abstract

The role of MR imaging for image-guided radiation therapy (IGRT) is becoming more and more important thanks to the excellent soft tissue contrast offered by MRI. Hybrid therapy devices with integrated MRI scanners are under active development for x-ray therapy. The combination of proton therapy with MRI imaging has only been investigated at the theoretical or conceptual level. Of concern is the deflection of the proton beam in the homogeneous magnetic field. A previous publication has come to the conclusion that the impact of a 0.5 T magnetic field on the dose distribution for proton therapy is very small and lateral deflections stay well below 2 mm. The purpose of this study is to provide new insights into the effects of magnetic fields on a proton beam coming to rest in a patient. We performed an analytical calculation of the lateral deflection of protons with initial energies between 50 MeV and 250 MeV, perpendicular to the beam direction and the magnetic field. We used a power-law range-energy relationship and the Lorentz force in both relativistic and non-relativistic conditions. Calculations were done for protons coming to rest in water or soft tissue, and generalized to other uniform and non-uniform media. Results were verified by comparisons with numerical calculations and Monte Carlo simulations. A key result of our calculations is that the maximum lateral deflection at the end of range is proportional to the third power of the initial energy. Accordingly, due to the strong dependence on the energy, even a relatively small magnetic field of 0.5 T will cause a deflection of the proton beam by 1 cm at the end of range of a 200 MeV beam. The maximum deflection at 200 MeV is more than 10 times larger than that of a 90 MeV beam. Relativistic corrections of the deflection are generally small but they can become non-negligible at higher energies around 200 MeV and above. Contrary to previous findings, the lateral deflection of a proton beam can be significant (1 cm and above) even in relatively small magnetic fields of 0.5 T. However, the curved path of a proton beam in a magnetic field is easily predictable and it should be possible to account for this in treatment planning.

(Some figures may appear in colour only in the online journal)

0031-9155/12/170329+09$33.00 Printed in the UK & the USA

1. Introduction

Proton therapy, while allowing for better dose conformality than photons due to the Bragg peak, is in practice limited by knowledge of patient anatomy at the time of treatment. Image-guided proton therapy allows taking full advantage of the Bragg peak's sharp distal dose falloff by precisely calibrating the beam energy to reach the known depth of the patient's tumour. Magnetic resonance imaging (MRI) is a noninvasive imaging method with a great ability to visualize patient anatomy. However, when used in combination with proton therapy, the MRI magnetic field causes the dose distribution to deform due to a lateral deflection of the Bragg peak. While this problem can be avoided by aligning the proton beam with the direction of the magnetic field, such an alignment may not be possible for the different beam orientations used in clinical treatments.

The main purpose of this study is to understand and quantify the deflection of protons, which come to rest at their end of range in matter or tissue. We will consider the realistic case in which the beam is perpendicular to the magnetic field. One of the questions is, does the slowing-down of the particles, and the resulting decrease of the radius of curvature, cause the trajectory to 'curl up'? Also, is the lateral deflection much bigger than that of particles that travel the same distance without losing energy?

Raaymakers *et al* used Monte Carlo methods to examine this effect for a 90 MeV proton beam (Raaymakers *et al* 2008). They found that a 0.5 T magnetic field produced only around 1 mm deflection in a simulated water phantom, and that even at 3 T the deflection was limited to 5 mm. However, an ideal hybrid proton MRI system in the future may need to work to energies above 200 MeV. While not yet technically feasible for such a hybrid system, this is the energy that clinical proton therapy systems now achieve. We note that the same group has since developed and tested prototype for a hybrid photon-MRI system at 1.5 T (Raaymakers *et al* 2009), indicating the feasibility of open MRI at larger field strengths. Also, 1 T open MRI machines exist on the market today. The 2008 study stated that at 0.5 T the magnetic deflection of a proton beam will never exceed 2 mm within the geometry of a human body, although this is contradicted by a later review article (Schippers and Lomax 2011) which indicated an 8 mm deflection at end of range for a 200 MeV beam in a 0.5 T field.

We developed a simple analytical approach to examine the trajectory of a slowing-down proton beam in a magnetic field. The approach is based on the power law range-energy relationship described in (Bortfeld 1997), where $R_0 = \alpha E_0^p$ for R_0 the range, E_0 the initial energy, and α and p power law fit parameters. Then the energy E varies as a function of the distance travelled s as

$$E(s) = \frac{1}{\alpha^{\frac{1}{p}}}(R_0 - s)^{\frac{1}{p}}. \tag{1}$$

With our approach we are able to replicate the deflections reported by Raaymakers *et al* , as well as provide our own numbers for the stopping position at end of range for an up to 250 MeV beam.

2. The analytical approach

For a charged particle such as a proton with velocity $v(s)$, kinetic energy $E(s)$, Lorentz factor γ, charge q, and rest mass m, which initially moves along the z-axis through a uniform magnetic field B pointing along the x-axis, the deflection angle ϕ between the particle motion and the z-axis satisfies

$$\frac{\mathrm{d}\phi}{\mathrm{d}s} = \frac{qB}{\gamma(s)mv(s)} = \frac{qB}{\sqrt{2mE(s)\left(1 + \frac{E(s)}{2mc^2}\right)}}, \tag{2}$$

where s is the distance the particle has travelled as measured along its curved path. By integrating over s we find the total deflection angle $\phi(s)$, as measured after the particle has travelled a distance s. This integration requires the functional form of $E(s)$, which is obtained from equation (1). For this paper we did a new fit of the power-law relationship $R_0 = \alpha E_0^p$ to the ICRU 49 range tables (ICRU 1993) for energies of 0 to 200 MeV in steps of 25 MeV, using the Matlab[1] curve fitting toolbox. When we saw that this resulted in $p \approx 1.75$, we set $p = 1.75$ and fitted the α, resulting in $\alpha \approx 2.43 \times 10^{-3}\text{MeV}^{-p}\text{cm}$ in water. The reason for this approach will become clear below. The fit is slightly better than our previous fit from (Bortfeld 1997) for higher energies: the range is within 1 mm for energies up to 200 MeV, and within 2 mm for energies up to 250 MeV. For tissue or media other than water, the value of α can be approximately obtained from the Bragg–Kleeman rule (Evans 1982, Bortfeld 1997). To first order, α can simply be scaled inversely with the electron density relative to water. For better accuracy, the value of p must also be adjusted due to the effect of the ionization potential on the relative stopping power.

Once $\phi(s)$ is known, the particle's lateral deflection, $y(s)$, can be computed by a second integration over s using the relationship $\mathrm{d}y/\mathrm{d}s = \sin\phi(s)$. The two integrations are straightforward to do numerically. Analytically, however, the integration for $\phi(s)$ is difficult to do in the relativistic model, and for $y(s)$ it may not be analytically possible. Therefore some approximations are necessary.

2.1. The non-relativistic case

We first considered a nonrelativistic model where $E(s) \ll 2mc^2$ such that the momentum in the denominator of equation (2) is $\sqrt{2mE(s)}$. With that, the integration of equation (2) over s using equation (1) is easy, resulting in

$$\phi(s) = \frac{2p}{2p-1}\frac{qB\alpha}{\sqrt{2m}}\left(E_0^{p-\frac{1}{2}} - E(s)^{p-\frac{1}{2}}\right). \tag{3}$$

When computing $y(s)$, further difficulties in integrability occur due to the sine, so we took a second order small angle approximation. Then $\mathrm{d}y/\mathrm{d}s \approx \phi(s)$, so that

$$y(s) = \int_0^s \phi(s')\,\mathrm{d}s'. \tag{4}$$

The two integrations to obtain $y(s)$ can in fact be combined through integration by parts, yielding:

$$y(s) = \frac{qB}{\sqrt{2m}}\int_0^s \frac{s-s'}{\sqrt{E(s')}}\,\mathrm{d}s'. \tag{5}$$

This can be seen by setting $u(s) = \phi(s)$ and $v' = 1$ and using the integration by parts rule $\int u(s)v'(s)\mathrm{d}s = u(s)v(s) - \int u'(s)v(s)\mathrm{d}s$, followed by replacing ϕ with the integral of equation (2).

In *homogeneous* media with $E(s)$ from equation (1), the integral can be solved without too much difficulty. Written in powers of the energy, it is

$$y(s) = \frac{qB\alpha^2 E_0^{2p-\frac{1}{2}}}{\sqrt{2m}}\left(\frac{2p}{4p-1} - \frac{2p}{2p-1}\left(\frac{E(s)}{E_0}\right)^p + \frac{4p^2}{(2p-1)(4p-1)}\left(\frac{E(s)}{E_0}\right)^{2p-\frac{1}{2}}\right). \tag{6}$$

[1] The MathWorks Inc., Natick MA, USA.

It is useful to note that for protons in a magnetic field of $B = 1\text{T}$, we have $qB/\sqrt{2m} = 0.0693\sqrt{\text{MeV}}\text{cm}^{-1}$. The maximum deflection near the end of range, $s = R_0$, is

$$y_{\max} = y(R_0) = \frac{2p}{4p-1}\frac{qB\alpha^2}{\sqrt{2m}}E_0^{2p-\frac{1}{2}} = \frac{7}{12}\frac{qB\alpha^2}{\sqrt{2m}}E_0^3. \tag{7}$$

The axial depth that the proton reaches will also be reduced due to the magnetic field. The depth satisfies $\mathrm{d}z/\mathrm{d}s = \cos\phi$ and so for small deflection angles ϕ, we can let $z(s) \approx s$. However, larger deflection angles at the end of range of higher energy particles necessitate using $\cos\phi \approx 1 - \phi^2/2$ so that

$$z(s) = s - \frac{1}{2}\int_0^s \phi^2(s')\,\mathrm{d}s', \tag{8}$$

which integrates to

$$z(s) = s - \frac{q^2B^2\alpha^3E_0^{3p-1}}{2m}\left(\frac{2p^2}{(4p-1)(3p-1)} - \frac{2p^2}{(2p-1)^2}\left(\frac{E(s)}{E_0}\right)^p + \frac{8p^3}{(2p-1)^2(4p-1)}\left(\frac{E(s)}{E_0}\right)^{2p-\frac{1}{2}} - \frac{2p^3}{(1-2p)^2(3p-1)}\left(\frac{E(s)}{E_0}\right)^{3p-1}\right). \tag{9}$$

2.2. A nonuniform geometry

With a small adjustment, we can treat a nonuniform geometry made up of layers of different materials. Suppose a slab extends from z_0 to z_1, and that the proton enters the slab travelling in the direction ϕ_0 with lateral deflection y_0. Then equation (3) gains a constant of integration and becomes

$$\tilde{\phi}(s) = \phi_0 + \phi(s) = \phi_0 + \frac{2p}{2p-1}\frac{qB\alpha}{\sqrt{2m}}\left(E_0^{p-\frac{1}{2}} - E(s)^{p-\frac{1}{2}}\right), \tag{10}$$

where E_0 is the energy the proton had when entering the layer, and α (and to a lesser degree p) is the property of this particular material. The path length s is now measured from the entrance of the slab and not from the beginning of the particle's motion. The deflection and depth now pick up extra terms due to the constants of integration, and become

$$\tilde{y}(s) = y_0 + \phi_0 s + y(s) \tag{11}$$

and

$$\tilde{z}(s) = z_0 - \phi_0 y(s) - \frac{\phi_0^2 s}{2} + z(s), \tag{12}$$

where $y(s)$ and $z(s)$ represent the homogeneous geometry solutions from equations (6) and (9).

Applying this layered model requires a functional form of $s(z)$ in order to determine the path length s travelled when the particle reaches the depth z_1 of the next boundary. At low energies, it is sufficient to use $s(z) = z$ so that the computation remains analytical. At higher energies where the next order angular corrections are necessary, the calculation of $s(z_1)$ must be done numerically.

With these equations we can treat a layered slab geometry of different materials. As an example we will consider the air gap geometry used in (Raaymakers *et al* 2008). Inside the air gap, we assume no attenuation of energy so that $\mathrm{d}\phi/\mathrm{d}s$ is constant. Then

$$\tilde{y}(s) = y_0 + \phi_0 s + \frac{qBs^2}{2\sqrt{2mE_0}} \tag{13}$$

and

$$\tilde{z}(s) = z_0 - \frac{qB\phi_0 s^2}{2\sqrt{2mE_0}} - \frac{\phi_0^2 s}{2} + s - \frac{q^2B^2s^3}{12mE_0}. \tag{14}$$

2.3. The relativistic case

In the more difficult relativistic case, there is a closed-form solution for the total deflection at $s = R_0$:

$$y_{\max} = \frac{qB}{\sqrt{2m}} \int_0^{R_0} \frac{R_0 - s'}{\sqrt{E(s')\left(1 + \frac{E(s')}{2mc^2}\right)}}\, \mathrm{d}s'. \tag{15}$$

From our range-energy relationship, equation (1), with $p = \frac{7}{4}$ we obtain $\mathrm{d}s' = -\frac{7}{4}\alpha E^{3/4}\, \mathrm{d}E$, and hence

$$y_{\max} = \frac{7}{4} \frac{qB\alpha^2}{\sqrt{2m}} \int_0^{E_0} \frac{E^2}{\sqrt{1 + \frac{E}{2mc^2}}}\, \mathrm{d}E. \tag{16}$$

This integral can be solved, yielding

$$y_{\max} = \frac{7}{30} \frac{qB\alpha^2}{\sqrt{2m}} (2mc^2)^3 \left[\sqrt{1 + \frac{E_0}{2mc^2}} \left(3 \left(\frac{E_0}{2mc^2} \right)^2 - 4 \left(\frac{E_0}{2mc^2} \right) + 8 \right) - 8 \right]. \tag{17}$$

Now a Taylor series expansion in E_0 yields

$$y_{\max} = \frac{7}{12} \frac{qB\alpha^2}{\sqrt{2m}} E_0^3 \left(1 - \frac{3}{8} \left(\frac{E_0}{2mc^2} \right) + \cdots \right) \tag{18}$$

so that in the nonrelativistic case, we recover equation (7).

Note that this solution exists only for $p = \frac{7}{4} = 1.75$, but not for the value of 1.77 that was used in (Bortfeld 1997), for example. This was part of the reason for re-doing the fit as mentioned above. Also, no closed-form solution has been found for $y(s)$ at $s < R_0$. Since the relativistic effect is small and becomes relevant only for higher energies at or above about 200 MeV, as we will show in the examples below, a simple pragmatic solution may be to scale the solution from equation (6), i.e. to multiply it by the factor $1 - \frac{3}{8}\left(\frac{E_0}{2mc^2}\right)$.

3. Examples of applications

In order to validate some of our approximations, we compared analytical trajectories to a simple numerical simulation. This simulation computed the forces on the proton using equations (1) and (2) and numerically integrated to find v, ϕ, y, and z. This served to elicit the effect of the small angle and nonrelativistic assumptions, which we found made a small but not always negligible difference in the stopping position. We considered 90 and 200 MeV beams in water, as well as the air gap geometry from (Raaymakers *et al* 2008) for a 90 MeV beam.

The stopping positions for each of these scenarios are shown in table 1. Notice that at 90 MeV, our nonrelativistic model matches the numerical calculation with submillimetre accuracy. At 200 MeV however, the analytical deflection is off by 3 mm. Using the relativistic deflection from equation (17) brings the 200 MeV stopping position back within 1 mm along both axes. The remaining discrepancy is due to the Taylor approximations of $\sin\phi$ and $\cos\phi$. Taking the nonrelativistic solution with a $1 - \frac{3}{8}\left(\frac{E_0}{2mc^2}\right)$ scale factor for the 200 MeV case gives a final deflection of $y = 5.49$ cm, which is within 0.2 mm of the fully relativistic endpoint.

The trajectories in water are plotted in figure 1. Because the curvature is highest near the proton's stopping point, the 90 MeV trajectory has a higher deflection than the 200 MeV trajectory at equivalent depth. However, because increasing energy increases the depth faster than the deflection, the maximum deflection is still larger at higher energies. The

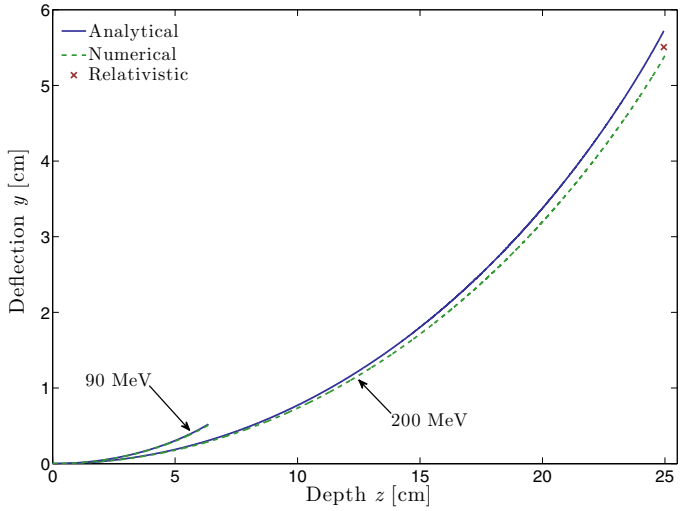

Figure 1. The trajectories of proton beams at 90 and 200 MeV are plotted for a 3 T magnetic field. Our nonrelativistic analytical model is plotted as well as a fully relativistic numerical simulation. The analytical relativistic endpoint is plotted in the 200 MeV case using equation (17). Note that axes are not to scale.

Table 1. End of range positions for different models and geometries. All reported numbers are for $B = 3$T.

Energy	Geometry	Model	y (cm)	z (cm)
90 MeV	Water	Numerical	0.51	6.36
		Analytical	0.52	6.36
	Air Gap	Numerical	0.86	8.33
		Analytical	0.88	8.33
200 MeV	Water	Numerical	5.41	25.02
		Analytical	5.72	24.95
		Analyt. (Rel.)	5.51	—

relativistic endpoint from equation (17) is also plotted, using the nonrelativistic depth from equation (9) for the z-coordinate.

Figure 2 compares the 90 MeV trajectories with and without an air gap. This was the geometry used in the previous study (Raaymakers *et al* 2008). Within the air gap, the proton has smaller curvature than it would in water, because it is no longer losing energy. However, similarly to the higher energy case, it still ends up with a larger final deflection because the air gap increases the range and leads to a larger final depth.

The previous examples assumed that the magnetic field edge is perfectly aligned with the water phantom. Figure 3 examines the case where there is nonzero field beginning at $z_B = -2$ cm in front of the phantom, for a 90 MeV beam. This causes a small deflection of 0.4 mm before the beam enters the water, and changes the entrance angle by 2.5°. At maximum depth, this increases the final deflection by 3.1 mm. This sensitivity to entrance phase space highlights the importance of correcting beam steering to account for the field even outside the patient.

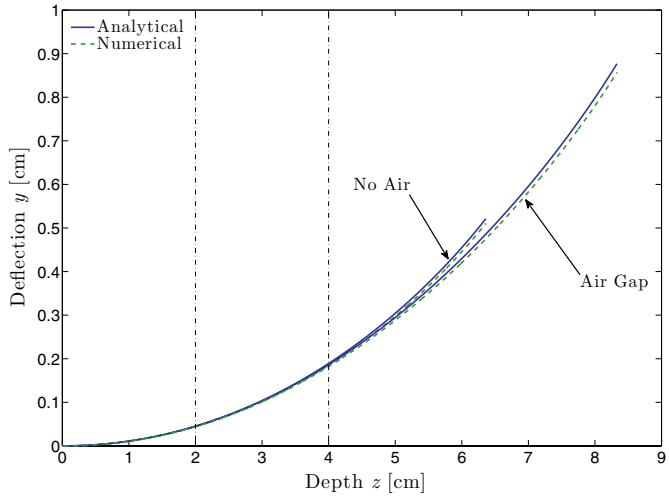

Figure 2. The trajectories of proton beams at 90 MeV with and without an air gap are plotted for a 3 T magnetic field. The air gap extends from $z = 2$ cm to $z = 4$ cm, as indicated by vertical lines. Our nonrelativistic analytical model is plotted as well as a fully relativistic numerical simulation. Note that axes are not to scale.

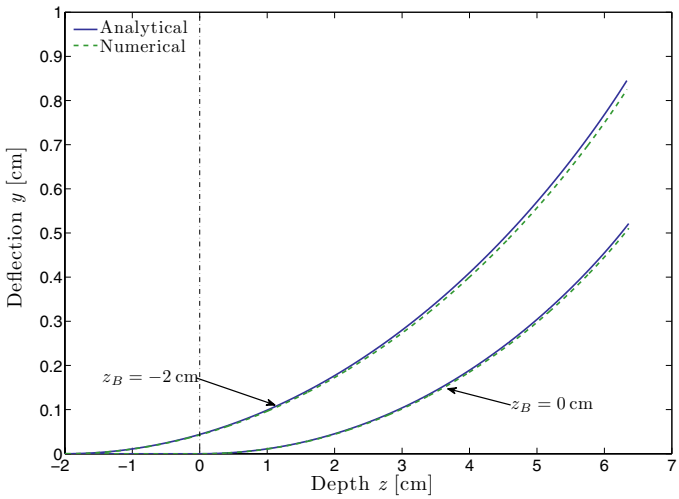

Figure 3. Trajectories for a 90 MeV beam with varying magnetic field starting position z_B. A field which extends 2 cm outside the water phantom results in a small deflection at the water entrance which grows to a much larger deflection at the Bragg peak. The surface of the water phantom is indicated by a vertical line at $z = 0$ cm. Note that axes are not to scale.

4. Discussion

Our main result is that the end-of-range displacement grows with the third power of the energy, shown in equations (7) and (17). While a 90 MeV beam in a 3 T field sees only a 5 mm lateral displacement of the Bragg peak, a 200 MeV beam sees greater than 5 cm deflection in water. This is certainly a significant effect which must be compensated for in MRI-guided proton therapy.

A similar effect is seen when considering the axially-projected depth. A 90 MeV beam in a 3 T magnetic field reaches a depth of 6.4 cm, which is equal to its total range at millimetre precision. However, for a 200 MeV proton the deflection has a measurable effect, as a 26.0 cm range translates to only a 25.0 cm depth. Thus although this effect is small, the magnetic field can necessitate a larger energy to reach an equivalent depth in tissue, which further impacts dose planning.

Of course, the relevance of these calculations hinges on the existence of hybrid proton-MRI systems at these fields and energies. Raaymakers *et al* note that current (as of 2008) systems are limited to 0.5 T due to mechanical issues. However, if the ultimate goal of such a hybrid MRI system is to replace current clinical proton therapy systems, then the dose deformation effects at large energy and field strength must be studied. It is clear from our calculations that very significant deflections (of the order of 1 cm) occur even at 0.5 T fields with energies around 200 MeV.

Even though particle energies become very small near the end of range, the particles do not 'curl up' in the magnetic field. This can be understood from the fact the slowing-down is so rapid that the residual range is not sufficient to cause a spiral-shaped trajectory. Incidentally, the rapid slowing down is the reason for the pronounced Bragg peak. It is also interesting to compare the lateral deflection from equation (7) with the deflection that would be experienced by a particle travelling the same distance without slowing down. The latter would be described by an equation with the same functional form as (7) but with a factor of $1/2$ instead of $7/12$. Thus, with slowing down the lateral deflection is only $1/6$ (17%) bigger than without.

In all our calculations it was assumed that the beam direction is perpendicular to the magnetic field. Other geometries can be considered simply by scaling the magnetic field strength with the direction cosine between the beam direction and the magnetic field.

While any analytic model will be inferior to numerical methods when it comes to dose planning in actual patients, our methods are useful in order to get a quick idea of the degree of correction needed to compensate for magnetic effects in a hybrid proton-MRI treatment system. We also believe that the analytical approach helps with the understanding of the underlying mechanisms and dependences of the effects. Furthermore, our simple analytical results such as equation (7) can serve as a reference solution, and it will be useful to compare any numerical calculations against them to detect any errors in the numerical results.

5. Conclusions

Our analytical model can estimate the deflection of a proton beam in an MRI magnetic field to good accuracy in a uniform or layered slab geometry. Using this model, we see similar numbers to (Raaymakers *et al* 2008) for the lateral beam deflection in water at 90 MeV and 3 T. Further, at a larger 200 MeV energy that is certainly clinically relevant in a future MRI-guided proton treatment system, we see a large deflection which must be accounted for in dose planning, as well as a small but significant range reduction. Useful rules of thumb resulting from our calculations are that in uniform media the total lateral deflection is proportional to the third power of the energy, and it is only 17% bigger than the deflection of a particle travelling the same distance without slowing down.

References

Bortfeld T 1997 An analytical approximation of the Bragg curve for therapeutic proton beams *Med. Phys.* **24** 2024–33

Evans R 1982 *The Atomic Nucleus* ed E Robert (Malabar, FL: Krieger)

ICRU 1993 Stopping powers and ranges for protons and alpha particles *International Commission on Radiation Units and Measurements Report ICRU 49* (Bethesda: MD: ICRU)

Raaymakers B, Raaijmakers A and Lagendijk J 2008 Feasibility of MRI guided proton therapy: magnetic field dose effects *Phys. Med. Biol.* **53** 5615–22

Raaymakers B W *et al* 2009 Integrating a 1.5 T MRI scanner with a 6 MV accelerator: proof of concept *Phys. Med. Biol.* **54** N229–37

Schippers J M and Lomax A J 2011 Emerging technologies in proton therapy *Acta Oncol.* **50** 838–50